



Structure-based insights into the ligand specificity tuning of 2'-dG-III riboswitch

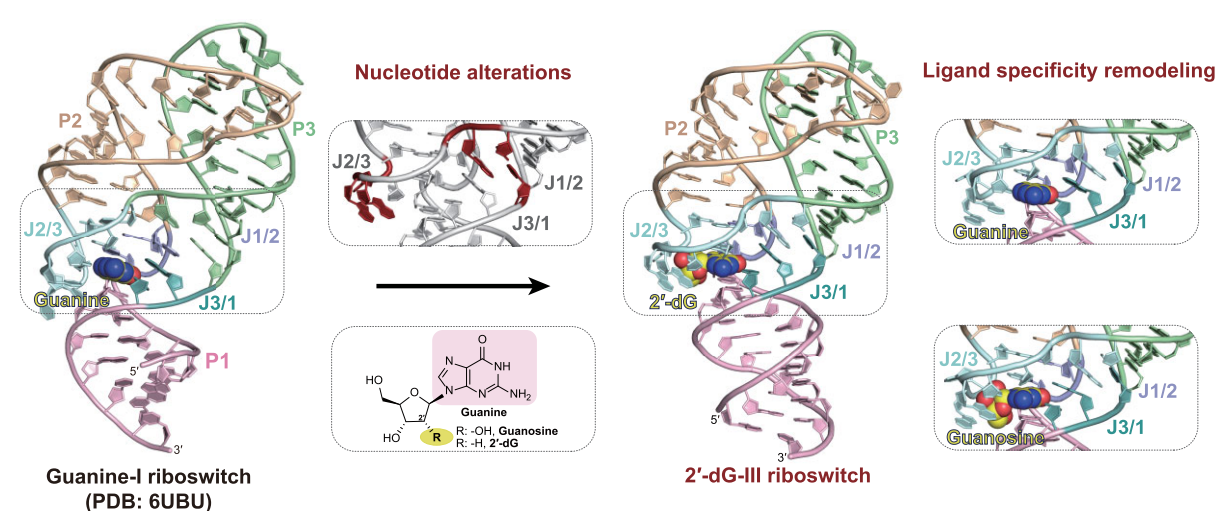
Xin Shen^{1,†}, Hongcheng Li^{1,†}, Xiaochen Xu^{1,2}, Qianqian Song¹, Xiaoqing Tai¹, Mengqi He¹, Aiming Ren ^{©1,*}

- ¹Department of Cardiology of The Second Affiliated Hospital and Life Sciences Institute and School of Medicine, Zhejiang University, Hangzhou 310058, China
- ²The Eighth Affiliated Hospital, Sun Yat-sen University, Shenzhen 518033, China
- *To whom correspondence should be addressed. Email: aimingren@zju.edu.cn
- [†]The first two authors should be regarded as Joint First Authors.

Abstract

Riboswitches are conserved non-coding RNA domains predominantly located at the 5'-end of the bacterial mRNAs, serving as gene expression regulators. Recently, a third class of 2'-deoxyguanosine riboswitch (2'-dG-III) has been identified from guanine riboswitch family, exhibiting comparable binding affinity toward 2'-dG, guanine, and guanosine. To elucidate the unique ligand recognition mechanism of this riboswitch, we solved its crystal structures in complex with different purine derivatives, including 2'-dG, guanine, and guanosine. The tertiary structure reveals a typical tuning-fork-like architecture, with three stems converging at a central three-way junction. The bound ligand, 2'-dG, is anchored within the junctional core through specific molecular interactions involving certain critical nucleotides. Through systemic comparative analysis of the binding pocket across different ligand-bound states, as well as related guanine family riboswitches, including 2'-dG-I, 2'-dG-II, and Guanine-I riboswitches, we identified subtle yet significant structural variations that modulate binding affinity and specificity. Leveraging these findings, we further engineered RNA biosensors by fusing the 2'-dG-III riboswitch with Pepper fluorogenic RNA aptamer, which exhibits a robust, positive correlation between fluorescence intensity and 2'-dG levels *in vitro*. Together, this work not only advances our understanding of the ligand recognition mechanisms underlying the 2'-dG-III riboswitch and related guanine riboswitch family but also lays the groundwork for fine-tuning riboswitch specificity, paving the way for the development of highly specific RNA-based biosensors.

Graphical abstract



Introduction

Riboswitches are RNA-based regulators of downstream gene expression, primarily located in the 5'-untranslated regions (5'-UTRs) of bacterial and archaeal mRNAs, with sporadic

reports in eukaryotes [1, 2]. Most riboswitches consist of two functional domains: a highly conserved sensing domain and an adjacent, variable expression platform. The sensing domain specifically recognizes and binds the cognate small molecule

Received: February 19, 2025. Revised: May 20, 2025. Editorial Decision: June 25, 2025. Accepted: July 24, 2025 © The Author(s) 2025. Published by Oxford University Press.

metabolite ligands, triggering conformational changes that alter the folding pattern of the expression platform. These structural changes, in turn, modulate the transcription or translation processes of downstream genes, therefore turning gene expression on or off [3-7]. Through this interplay between the sensing domain and the expression platform, riboswitches dynamically regulate gene expression related to cellular metabolism in response to the fluctuating concentrations of their cognate metabolite [8-10]. Since the discovery of riboswitches in 2002, over 55 types of riboswitches have been identified [11]. Based on their cognate ligands, riboswitches have been classified into different classes, including those sensing coenzymes, purines and their derivatives, signaling molecules, amino acids, ions, and others [11]. The diversity of riboswitches indicates their essential role in maintaining cellular homeostasis and adapting to dynamic changes across a wide range of metabolic pathways.

Among known riboswitches, the purine and purine-derived riboswitch family is phylogenetically widespread in bacteria. These riboswitches specifically interact with ligands containing purine chemical structures, such as adenine, guanine, xanthine, and 2'-dG [12], playing a crucial role in maintaining cellular purine metabolism by dynamic regulation of the biosynthesis, transport, and degradation of purines and derivatives in bacteria [13]. Although guanine and adenine riboswitches both adopt a three-way junction fold with similar overall tertiary architecture, a single mutation of C-to-U in the ligandbinding pocket can switch the ligand specificity from guanine to adenine [14]. In addition, subsequent research has demonstrated that minor alterations within the core of the binding pocket can significantly influence ligand recognition, enabling guanine riboswitches to exhibit varied specificities. Notably, several variants of the guanine riboswitch family have been identified as new riboswitch classes, highlighting the evolutionary adaptability and functional diversity of these RNAbased regulators [14–17].

In 2007, the first 2'-dG riboswitch, termed the 2'-dG-I riboswitch [15], was identified primarily in Mesoplasma florum. This riboswitch exclusively binds to 2'-dG and regulates the expression of downstream ribonucleotide reductase genes [15]. Subsequently, in 2017, a variant of the guanine riboswitch (UCC group), discovered in environmental samples, was found to recognize 2'-dG as its natural ligand and was classified as the 2'-dG-II riboswitch [16]. More recently, a new variant of the guanine riboswitch was identified in Bacillus species [17]. In-line probing analysis revealed that, unlike canonical guanine riboswitches, this variant exhibits reduced affinity for guanine but retains low micromolar binding affinity for 2'-dG. This riboswitch regulates the expression of a downstream gene encoding purine nucleoside phosphorylase, suggesting its role in modulating gene expression in response to nucleoside levels. Compared to 2'-dG-I and 2'-dG-II riboswitches [18, 19], this variant shares a similar three-way junction structure but features a unique sequence within its binding pocket, leading to the designation as the 2'-dG-III riboswitch [17] (Supplementary Fig. S1A and B).

Despite these discoveries, the mechanisms by which mutations in the core binding pocket fine-tune binding affinity and specificity remain unclear. Deciphering these intricate principles will not only deepen our understanding of how RNA recognizes small molecules with different modifications but also provide valuable insights into the discovery of new classes of

riboswitches. As previously mentioned, purines play important roles in cellular metabolism and function. The development of robust and sensitive biosensors capable of spatiotemporal tracking of purines and their derivatives holds significant promise for advancing the study of purine metabolism with high precision. Investigations into the tertiary structures of purine and purine-derivative riboswitches, which act as sensing modules, and fluorogenic RNA aptamers, which serve as signaling modules, provide essential information for designing RNA-based biosensors.

To elucidate the overall folding of the 2'-dG-III riboswitch, we employed X-ray crystallography to determine its tertiary structure. We successfully solved the crystal structure of the 2'-dG-III riboswitch in complex with 2'-dG at a high resolution of 2.1 Å, revealing the unique composition of its ligand binding pocket. Furthermore, we solved the structures of the 2'-dG-III riboswitch bound to guanine and guanosine, respectively. Comparative analyses of these structures, combined with systematic mutational analysis of the 2'-dG-III riboswitch and isothermal titration calorimetry (ITC) experiments, provided crucial insights into the molecular basis of ligand selectivity for the 2'-dG-III riboswitch. Additionally, we also conducted a detailed comparison of the junction regions of 2'-dG-III riboswitch with those of 2'-dG-I/II riboswitches and the Guanine-I riboswitch, shedding light on the molecular mechanisms that fine-tune their differences in ligand selectivity and binding affinity. Based on these structural and mechanistic insights, we fused the 2'-dG-III riboswitch with the Pepper aptamer, a well-characterized fluorogenic RNA element. By fine-tuning the ligand specificity of the 2'-dG-III riboswitch, we developed an RNA-based sensor capable of detecting 2'-dG levels with enhanced sensitivity and specificity.

Materials and methods

RNA preparation

To facilitate in vitro transcription, specific nucleotides (5'-GG and 3'-UC) were introduced into stem P1 of 2'-dG-III riboswitch. Subsequently, the complete sequence, followed by a self-cleaving hammerhead ribozyme, was cloned into the pUT7 vector, which contained a T7 RNA polymerase promoter [20]. The DNA templates for *in vitro* transcription were then amplified on a large scale by polymerase chain reaction. In vitro transcription was performed using T7 RNA polymerase at 37°C for 4.5 h. The resulting transcript was isolated by urea-denatured polyacrylamide gel electrophoresis (8 M urea-PAGE) and the target RNA was extracted from the gel by soaking in $0.5 \times \text{Tris-Acetate-EDTA}$ (TAE) buffer at 4°C . Following extraction, the RNA was further precipitated using isopropanol method, washed with 80% ethanol, and ultimately dissolved in diethyl pyrocarbonate (DEPC)-treated, double-distilled water.

Ligands

2'-Deoxyguanosine, guanine, 3'-deoxyguanosine, guanosine 5'-phosphate, xanthine, hypoxanthine, adenine, and 2'-deoxyadenosine were purchased from Yuanye Bio-Technology Co. Ltd. (Shanghai). Adenosine was purchased from Sigma–Aldrich. Guanosine was purchased from Macklin.

Crystallization

The purified RNA was dissolved in a buffer containing 40 mM HEPES (pH 7.4), 50 mM KCl, and 5 mM MgCl₂ at a concentration of 0.4 mM. The RNA sample was annealed at 65°C for 5 min, then cooled on ice for half an hour. The ligand was subsequently added to a final concentration of 4 mM and incubated with the RNA on ice for an additional 30 min. Crystallization trials were conducted using the sittingdrop diffusion method by mixing the RNA-ligand complex with the well solution at a 1:1 ratio, followed by incubation at 16°C. Well-diffracted crystals of 2'-dG-III riboswitch bound to 2'-dG grew within 2 days under conditions containing 0.08 M Sodium chloride, 0.012 M Potassium chloride, 0.02 M Magnesium chloride hexahydrate, 0.04 M Sodium cacodylate trihydrate, pH 7.0, 30%-35% v/v (±)-2-Methyl-2,4-pentanediol, and 0.012 M Spermine tetrahydrochloride. Crystals of the 2'-dG-III-D4 riboswitch bound to guanosine or guanine also grew under similar conditions. All crystals were cryoprotected using the well solution and flash-frozen in liquid nitrogen.

X-ray diffraction data collection and structure determination

All the crystals were flash-frozen using liquid nitrogen and transported to the Shanghai Synchrotron Radiation Facility (SSRF), where the X-ray diffraction data were collected at beamlines BL18U1 and BL02U1. The diffraction data were subsequently processed utilizing the XDS program [21]. The phase problem of 2'-dG-III riboswitch bound to guanosine was solved by molecular replacement using the Phaser MR program in the CCP4 suite with reported Guanine-I riboswitch (PDB: 1Y27) [22] as an initial structure model [23]. The structure model was further built and refined by Coot [24] and Phenix programs [25]. Additionally, the structures of the 2'-dG-III riboswitch bound to either 2'-dG or guanine were determined by the molecular replacement method, with the 2'-dG-III riboswitch-guanosine structure serving as the initial model. The detailed statistics of the crystal diffraction data and structure refinement are provided in Supplementary Tables S1 and S2.

Isothermal titration calorimetry

The ITC experiments were conducted on ITC-200 microcalorimeter or MicroCal PEAQ-ITC calorimeter at the National Center for Protein Science Shanghai (NCPSS). The purified RNAs were dialyzed overnight at 4°C in an ITC buffer containing 40 mM HEPES (pH 7.4), 50 mM KCl, and 10 mM MgCl₂. To investigate the effects of MgCl₂ concentration on the affinity of the 2'-dG-III riboswitch for 2'-dG, the RNAs were dialyzed in a buffer containing 40 mM HEPES (pH 7.4) and 50 mM KCl, supplemented with MgCl₂ at varying concentrations ranging from 0 to 20 mM. Subsequently, to further investigate the impact of different divalent metal ions, separate dialysis experiments were conducted using ITC buffers in which MgCl₂ was replaced with 10 mM of CaCl₂, BaCl₂, or MnCl₂, respectively. After dialysis, the RNA samples were diluted to the concentration of 0.05 mM for 2'dG and guanosine, and to 0.18 mM for guanine. They were then refolded by heating at 65°C for 5 min, followed by rapid cooling on ice for 30 min prior to the titration. Ligands were dissolved in their respective dialysis buffer at final concentrations of 0.5 mM for 2'-dG and guanosine, and

0.018 mM for guanine. During titration, an initial 0.4 μ L injection of the prepared 2′-dG or guanosine solution was administered into 200 μ L of RNA sample in the cell, followed by 18 serial 2 μ L injections with 2 min intervals. The reference power was set to 5 μ cal s⁻¹. For guanine, the procedure was reversed, with the RNA titrated into the ligand solution. Integrated heat data were analyzed using a one-site binding model through the MicroCal PEAQ-ITC Analysis Software. All the thermodynamic binding parameters are presented in Supplementary Table S3.

In vitro characterization of 2'-dG sensors

The RNA-based sensors were transcribed in vitro using T7 RNA polymerase and purified through 8 M urea-PAGE, followed by isopropanol precipitation. The RNA samples were prepared in a buffer containing 40 mM HEPES (pH 7.4), 50 mM KCl, and 1 mM MgCl₂ at a final concentration of 1 μM. To ensure proper folding, the RNAs were first denatured by heating at 65°C for 5 min, followed by a 30 min cooling on ice. Then, varying concentrations of ligand were added to the RNA samples, resulting in RNA-to-ligand molar ratios ranging from 1:0 to 1:10 000. The mixtures were then incubated on ice for 30 min. Afterward, 5 µM of the HBC fluorophore was added to each sample, followed by an additional 30 min incubation at 25°C to ensure complete binding. Fluorescence signal was measured using a Synergy Neo2 Multi-Mode Microplate Reader (BioTek) with an excitation wavelength of 485 nm (± 20 nm) and an emission wavelength of 530 nm (± 20 nm) for HBC. All fluorescence experiments were independently repeated three times to ensure reproducibility.

Results and discussion

Crystallization and tertiary structure of 2'-dG-III riboswitch in complex with 2'-dG

The previously reported 2'-dG-III riboswitch is predominantly found in B. species, and the sequences identified are highly conserved [17] (Chemical structure of 2'-dG depicted in Fig. 1A). Its consensus secondary structure consists of three stems (P1, P2, and P3) connected by a three-way junction (J1/2, J2/3, and J3/1), consistent with the featured overall architecture of guanine riboswitches (Supplementary Fig. S1A-C). The specific sequences (CAA) that substitute the original sequence (UYUC), as well as the insertion sequences (A42, U43, and U61) in the central junction region, have been highlighted with red shading [17] (Fig. 1B and Supplementary Fig. S1B and C). To minimize unexpected structural alterations resulting from additional mutations, we preserved the majority of the wild-type (WT) 2'-dG-III riboswitch sequence, while incorporating a 5'-GG in stem P1 to facilitate in vitro transcription and varying the length of stem P1 for crystallization trials. After screening a large number of RNA constructs for crystallization, a 73-nucleotide long RNA complexed with 2'-dG yielded high-quality crystals with a well-diffracting resolution of 2.1 Å (Fig. 1B). The space group is C121, and each asymmetric unit contains one molecule (Supplementary Table S1). The phase problem was solved by molecular replacement method, using one stem-loop from guanine riboswitch (PDB:1Y27) as the initial structure model [22]. The binding affinity of the 2'-dG-III riboswitch to 2'-dG is determined using ITC, generating a dissociation constant K_d amounting to 2.6 \pm 0.1 μM

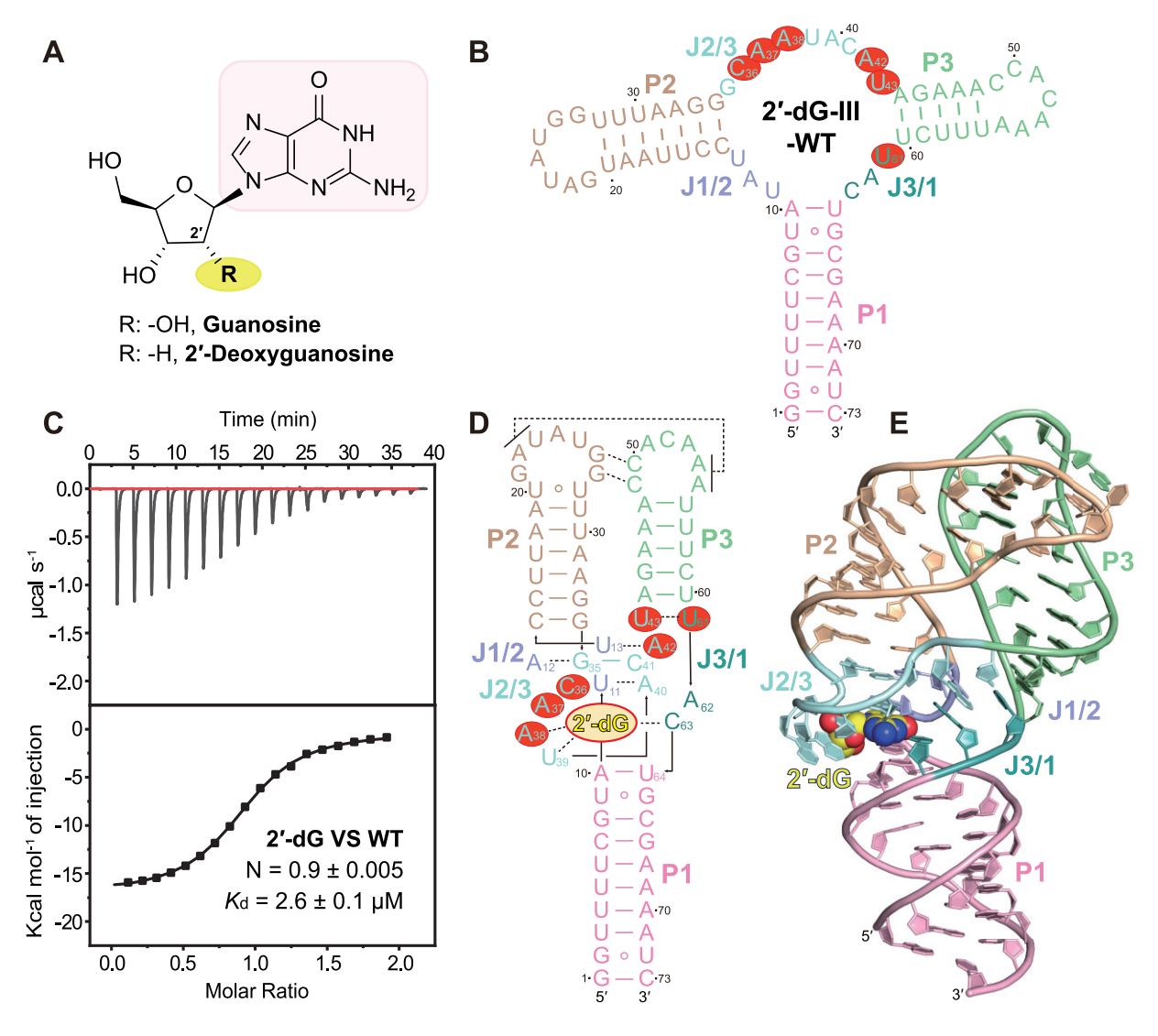


Figure 1. Secondary and tertiary structure of 2'-dG-III riboswitch bound to 2'-dG. (**A**) Chemical structure of 2'-dG and guanosine with the guanine moiety highlighted in pink. The 2'-residue is framed in yellow. (**B**) The secondary structure of the 2'-dG-III riboswitch. The nucleotides in the junction region that differ from those in the Guanine-I riboswitch are highlighted in red. Different regions are color-coded consistently with the corresponding regions in the cartoon representation shown in panel (E). (**C**) ITC experiment showing the binding of the 2'-dG-III riboswitch (WT) to 2'-dG. (**D**) Schematic representation of the tertiary structure of the 2'-dG-III riboswitch in complex with 2'-dG. Compared to the Guanine-I riboswitch, nucleotide changes in the junction region are highlighted in red. Long-distance interactions are depicted as dashed lines. Different regions are color-coded consistently with the corresponding regions in the cartoon representation shown in panel (E). (**E**) Cartoon representation of the overall structure of the 2'-dG-III riboswitch bound to 2'-dG.

and a binding stoichiometry close to 1:1. The thermodynamic parameters were estimated as $\Delta H = -16.9 \pm 0.2$ kcal/mol and $\Delta G = -7.6$ kcal/mol (Fig. 1C, Supplementary Fig. S2A and B, and Supplementary Table S3). In the following description, this construct is defined as WT compared with other mutants in ITC experiment.

The tertiary structure of the 2'-dG-III riboswitch is depicted schematically in Fig. 1D and illustrated as cartoon representation in Fig. 1E. The overall structure adopts a tuning fork-like configuration, with stem P1 (in light pink) serving as the handle, while stems P2 (in wheat) and P3 (in pale green) extend outward as the prongs (Fig. 1D). These three stems are connected through a central junction, which is subdivided into three distinct parts: J1/2 (in slate), J2/3 (in pale cyan), and J3/1 (in deep teal). Stem P1 connects to stems P2 and P3 through junction regions J1/2 and J3/1, respectively, while P2 and P3 are linked by junction region J2/3. Above the junction,

stems P2 and P3 twist and gradually converge toward each other along the central axis.

It was noted that three junction regions, J1/2, J2/3, and J3/1, all gather in the middle of the tertiary structure and are intricately organized, constituting the core domain of 2'-dG-III riboswitch (Fig. 1D and E). Most nucleotides within the junctions participate in continuous stacking interactions, contributing to the structural stability of the riboswitch. Meanwhile, certain nucleotides within J2/3 flip their bases downward to form a specialized ligand-binding pocket (Fig. 1D and E). This central pocket securely accommodates the bound ligand, 2'-dG, which plays a crucial role in the riboswitch's regulatory function (Fig. 1D and E). At the apex of the overall structure, P2 and P3 establish complex long-range interactions (Supplementary Fig. S3A-C). Specifically, A22 and A55 engage in a Watson-Crick/Hoogsteen base pair, while G27 and C49 form a Watson-Crick base pair. Additionally, A55 and

G27 interact via a trans Watson-Crick/sugar-edge pairing, collectively constituting an A22-A55-G27-C49 base quadruple (Supplementary Fig. S3D). Stacked above this assembly, G26 and C50 form a canonical Watson-Crick base pair, while U23 and A54 engage in a Watson-Crick/Hoogsteen base pair. The 2-NH₂ group of G26 forms an additional hydrogen bond with the O2 of U23, and concurrently, the sugar edge of C50 forms two hydrogen bonds with the Watson-Crick edge of A54. Together, these interactions stabilize and reinforce the second base quadruple, U23-A54-C50-G26 (Supplementary Fig. S3E). The two quadruples are also interconnected through hydrogen bonds involving the 2'-OH of G26, which interacts with both the 2'-OH and N3 of A22 (Supplementary Fig. S3F). Above the U23-A54-C50-G26 tier, A53 and A24 form a Watson-Crick/Hoogsteen base pair (Supplementary Fig. S3G). At the top of the loop, the two consecutive nucleotides A51 and C52 adopt a coplanar arrangement, which is stabilized by a hydrogen bond between the 4-NH₂ of C52 and the N3 of A51. Besides, two hydrogen bonds are formed between the 2'-OH of A24 and the Watson-Crick edge of A51. A further hydrogen bond is established between the phosphate-oxygen of A24 and the 4-NH₂ group of C52. Moreover, the N3 of C52 engages in a hydrogen bond with the 2'-OH of U23 (Supplementary Fig. S3G). In addition, within stem P2, U20 forms a trans Watson-Crick base pair with U28, thereby increasing the number of base pairs in this region (Supplementary Fig. S3H). ITC experiments reveal that mutating the base pairing of A22-A55 and U23-A54 reduces the riboswitch's binding capacity for 2'-dG, while disrupting the complementary base pairs G26-C50 and G27-C49 completely abolishes the binding affinity (Supplementary Figs S3I and S4A and B, and Supplementary Table S3). These observations suggest that the long-distance interactions among these base pairs form a cohesive network that bridges the distal ends of the stems, thereby enhancing the stability of the overall structure.

Junctional folding in the 2'-dG-III riboswitch

In the 2'-dG-III riboswitch tertiary structure, nucleotides from the three segmented junction regions (J1/2, J2/3, and J3/1) form a network of long-range base-stacking and hydrogenbonding interactions (Figs 1D and 2A). These interactions not only enhance the overall structural stability of the riboswitch, but also contribute to the formation of a ligand-binding pocket. In the J2/3 region, five consecutive nucleotides (A37 to C41) are stacked successively, collectively forming the structural scaffold to support the ligand-binding pocket (Fig. 2A). It is found that C36 adopts an outwardly flipped conformation and does not participate in the pocket formation. J1/2 region consists of three nucleotides (U11, A12, and U13), which form intricate hydrogen bonding interactions with specific nucleotides in J2/3 region. U11 (J1/2) and A40 (J2/3) form one Watson-Crick base pair, positioned as the first tier stacked above 2'-dG (Fig. 2B). A12 (J1/2) extends toward J2/3 and forms two hydrogen bonds through its Watson-Crick edge with the minor groove of G35 (J2/3). Meanwhile, G35 and C41 (J2/3) form another Watson-Crick base pairing interaction. Consequently, a base triple is formed in the second tier (Fig. 2C). U13 (J1/2) engages in a Watson-Crick/Hoogsteen edge interaction with A42 (J2/3) and is positioned above A12 (J1/2) while oriented in the opposite direction (Fig. 2A). Herein, the U13-A42 base pair is sandwiched between a single

nucleotide, A62, and a non-canonical base pair, U43-U61 (Fig. 2D). Notably, U43 is the last nucleotide of J2/3, and U61 is the first nucleotide of J3/1. U43-U61 constitutes the final base pair preceding stem P3, playing a pivotal role in bridging the junction and stabilizing the riboswitch structure (Fig. 2A).

To further validate our observation in 2'-dG-III riboswitch crystal structure, we introduced mutations into the relevant nucleotides and employed ITC experiments to investigate the influence of these base interactions on the riboswitch's binding affinity for 2'-dG under the same conditions (Fig. 2E). U11 and A40 form a canonical Watson-Crick base pair, and mutations of U11 to either A11 or G11 (U11A or U11G) are not tolerated (Fig. 2E and Supplementary Table S3). Additionally, A12, G35, and C41 constitute a base triple interaction. Disruption of this base triple, particularly through mutations such as G35C-C41G, G35C, or G35A-C41U, results in a significant decrease or complete loss of binding activity (Fig. 2E, Supplementary Fig. S4C, and Supplementary Table S3). These findings underscore the importance of the intricate long-distance interactions within the junction region in maintaining the tertiary structure of the riboswitch and enabling the formation of the ligand-binding pocket. However, the single mutation C41G only slightly reduces the binding affinity for 2'-dG by 2.5-fold (Fig. 2E, Supplementary Fig. S4D, and Supplementary Table S3). Similarly, introducing U13G and U43C mutations to disrupt the pairing interaction of A42-U13 and U43-U61 in the junction also has a minor impact on binding affinity, causing 6.0-fold and 1.7-fold reductions, respectively (Fig. 2E, Supplementary Fig. S4E and F, and Supplementary Table S3). These results may be attributed to compensatory interactions formed by mutations of C41G, U13G, and U43C, including alternative hydrogen bonding or base-stacking interactions with adjacent nucleotides. Such compensatory effects highlight the limited yet adaptable structural flexibility of the 2'-dG-III riboswitch, which allows it to retain partial binding functionality despite local disruptions in base pairing.

In the structure of 2'-dG-III riboswitch bound to 2'-dG, a magnesium ion was observed adjacent to stem P1, specifically located on the exterior of the phosphate backbone between U9 and A10 below J1/2 region (Supplementary Fig. S5A and B). To investigate the impact of Mg²⁺ on the binding affinity of the 2'-dG-III riboswitch for 2'-dG, we conducted ITC experiments under varying Mg²⁺ concentrations (ranging from 0 to 20 mM). As shown in Fig. 2F, no detectable binding affinity was observed at concentrations of 0.5 mM or below. At 1 mM of Mg²⁺, weak affinity was detected, which increased with the presence of higher Mg²⁺ concentrations. However, beyond 5 mM of Mg²⁺, the affinity reached a plateau and showed no further significant enhancement. The measured binding affinity K_d was as follows: $8.1 \pm 0.2 \,\mu\text{M}$ at $2 \,\text{mM MgCl}_2$, 3.4 ± 0.1 μM at 5 mM MgCl₂, 2.9 \pm 0.1 μM at 10 mM MgCl₂, and $3.0 \pm 0.1 \,\mu\text{M}$ at 20 mM MgCl₂ (Supplementary Fig. S5C– H and Supplementary Table S3). These results indicate that Mg²⁺ plays a crucial role in promoting the riboswitch's ligand affinity by neutralizing the negative charges of the phosphate backbone and facilitating proper riboswitch folding.

To further examine the impact of various divalent metal ions on the binding affinity of the 2'-dG-III riboswitch, Mg²⁺ was substituted with other divalent metal ions, including Ca²⁺, Ba²⁺, and Mn²⁺. ITC experiments at a concentration of 10 mM demonstrated that neither Ca²⁺ nor Mn²⁺ significantly affected the binding affinity compared to Mg²⁺.

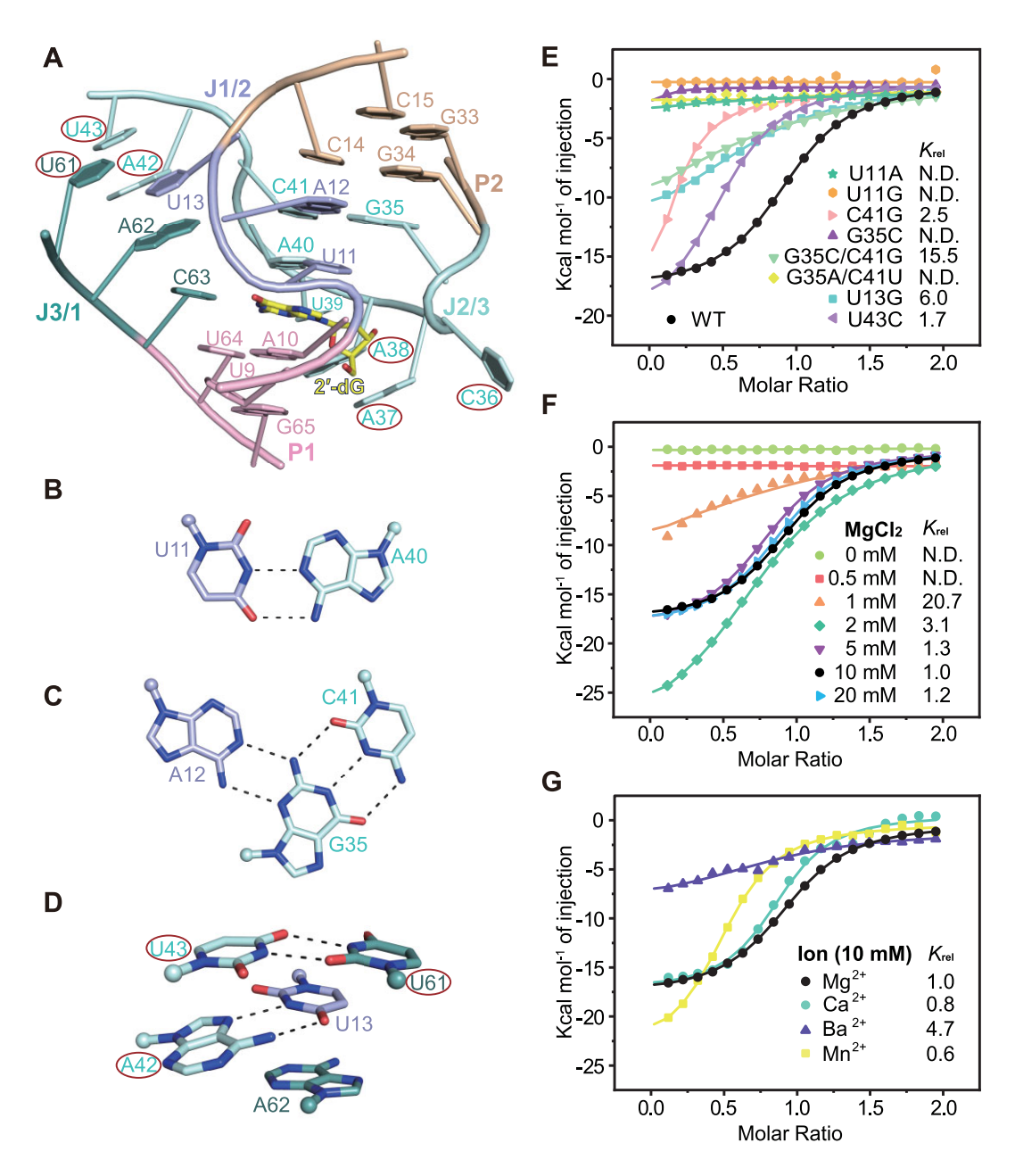


Figure 2. Long-distance interactions within junction regions of the 2'-dG-III riboswitch. (A) An expanded view highlights three junction regions that refine the binding pocket. The distinct inserted and mutated nucleotides C36, A37, A38, A42, U43, and U61 of Guanine-II riboswitch, which differ from the conserved nucleotides in the Guanine-I riboswitch, are framed in red. (B) A40 (J2/3) and U11 (J1/2) form a canonical Watson–Crick base pair, with hydrogen bonds depicted as black dashed lines. (C) A base triplet interaction is formed by A12 (J1/2), G35 (J2/3), and C41 (J2/3). (D) A close-up view of two types of long-distance interactions in the junction region: a Watson–Crick/Hoogsteen edge interaction formed between U13 and A42, and a non-canonical base pair formed by U43 and U61. Additionally, the A42-U13 base pair is sandwiched between the U43-U61 base pair and a single A62. (E) Overlay of the fitted integrated heat plots from ITC experiments between WT and mutants that disrupt interactions within long-distance junctions. (F) Overlay of the fitted integrated heat plots obtained from ITC experiments investigating the impact of various concentrations of Mg²+ on the binding of 2'-dG-III riboswitch to 2'-dG in equal concentrations of Mg²+, Ca²+, Mn²+, and Ba²+. K_{rel} represents the ratio of the average binding affinity of the mutants to 2'-dG relative to that of the WT.

However, the presence of 10 mM Ba²⁺ notably reduced the binding affinity (Fig. 2G, Supplementary Fig. S6A–C, and Supplementary Table S3). This reduction is presumably attributed to the larger ionic radius and lower charge density of Ba²⁺, which weaken its interactions with neighboring residues. These results suggest that the 2'-dG-III riboswitch exhibits a selective dependency on specific divalent metal ions.

Composition of 2'-dG binding pocket in 2'-dG-III riboswitch

The surface representation of the 2'-dG-III riboswitch binding pocket is shown in Fig. 3A, with the bound 2'-dG embedded within a cavity formed by the continuous stacking of nucleotides within the junction region and the apex of P1. A detailed close-up view of the binding pocket, depicted

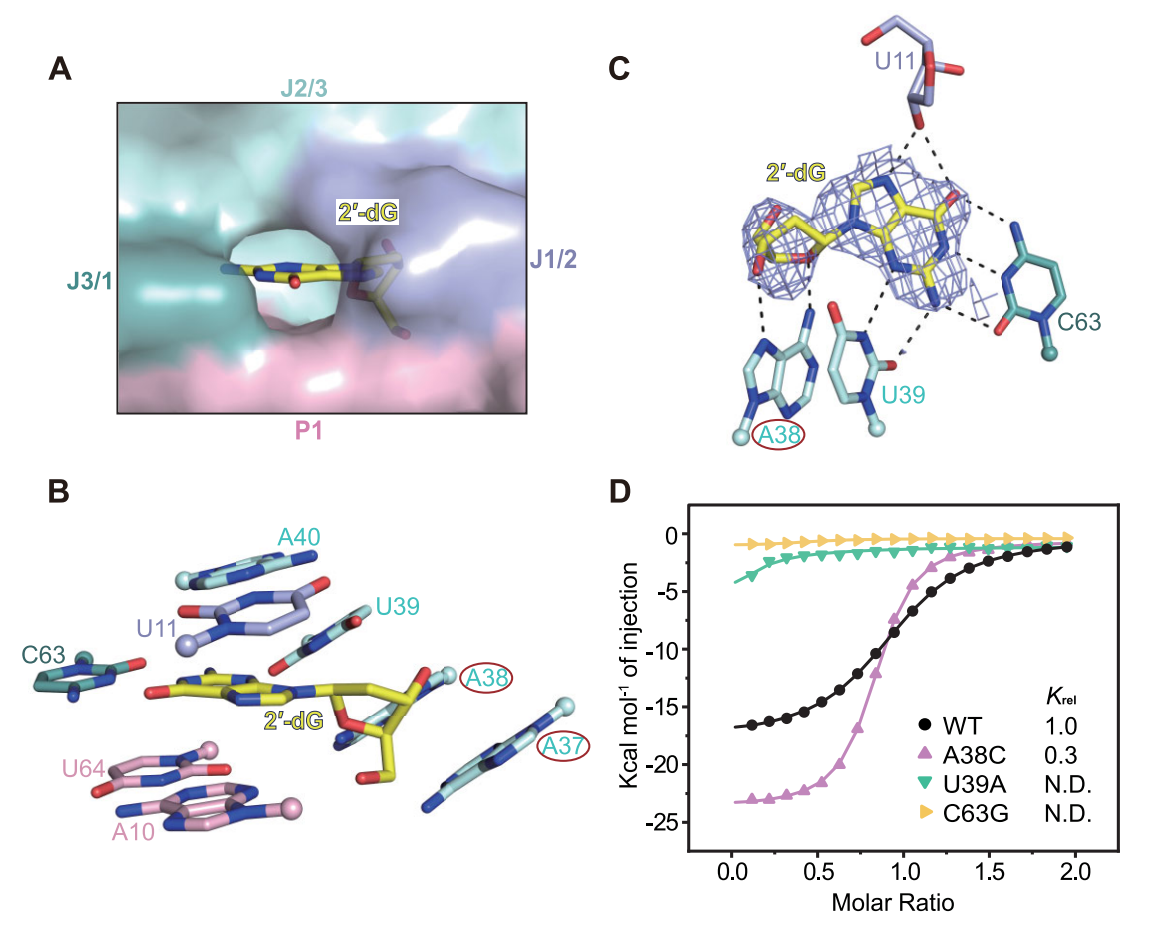


Figure 3. Structural details of 2'-dG interacting with 2'-dG-III riboswitch. (A) Surface representation of the ligand-binding pocket. The 2'-dG is buried within a cavity formed by the upper segment of P1 and the junction region. (B) A close-up view of the bound 2'-dG and its surrounding nucleotides shown as stick representations. 2'-dG forms a canonical Watson–Crick base pair with C63, which is further sandwiched between U11-A40 and A10-U64. The distinct mutated nucleotides A37 and A38 of Guanine-II riboswitch are framed in red. (C) Detailed view of the residues involved in hydrogen bonding interactions with 2'-dG. The composite omit electron-density map of 2'-dG, contoured at the 1.0 σ level, is shown in slate. (D) Overlay of the fitted ITC integrated heat plots of WT and mutants that change the residue interaction within binding pocket. K_{rel} represents the ratio of the average binding affinity of the mutants to 2'-dG relative to that of the WT.

in Fig. 3B (shown in stick representation), reveals the precise interactions that stabilize the bound ligand. The base of 2'-dG is sandwiched between the base pairs A10-U64 and U11-A40, forming a stable framework. Furthermore, 2'-dG molecule engages in additional base pairing interaction with the Watson-Crick edge of C63, the Watson-Crick edge of U39, and the sugar of U11 via its Watson-Crick, sugar, and Hoogsteen edges, respectively (Fig. 3B and C, shown in stick). Notably, the Hoogsteen edge of A38 forms two additional hydrogen bonds with the furan oxygen and the 3'-OH of the 2'dG ribose (Fig. 3C). Alongside the bound 2'-dG, nucleotides U39, A38, and A37 from the I2/3 region exhibit a continuous stacking arrangement beneath the A40-U11 base pair, providing a structural "bracket" that partially envelopes the bound 2'-dG and stabilizes the bound state (Fig. 3B). Interestingly, C36 is located near the ribose moiety of the 2'-dG but is partially disordered and does not participate in any direct interactions with the ligand (Fig. 2A). Instead, A38 and U39 significantly contribute to stabilizing the conformation of the bound 2'-dG by stacking on each other and forming hydrogen bond interactions with the ribose and the base of 2'-dG, respectively. The calculated $2F_{\text{observe}} - F_{\text{calculate}} (2F_{\text{o}} - F_{\text{c}})$ composite omit electron density map of the bound 2'-dG is shown

at 1.0 σ level in Fig. 3C. These interactions collectively anchor the bound 2'-dG.

Subsequent ITC experiments were employed to validate our structural observations in the ligand binding pocket of 2'-dG-III riboswitch (Fig. 3D and Supplementary Table S3). The C63G mutation, which disrupts the canonical Watson–Crick base pairing interaction formed between C63 and 2'-dG, abolishes the binding affinity for 2'-dG. Similarly, mutation of U39 to A (U39A) abolishes the riboswitch's binding affinity, emphasizing the importance of U39 in ligand stabilization. In contrast, when A38 was mutated to C (A38C), the binding affinity for 2'-dG increased, potentially due to the retention of certain hydrogen bond interactions or the formation of alternative stabilizing interactions with adjacent residues (Fig. 3D, Supplementary Fig. S6D, and Supplementary Table S3).

These findings underscore the critical role of the intricate hydrogen bonding network and nucleotide stacking interactions in maintaining the structural integrity of the binding pocket and stabilizing 2'-dG within the riboswitch. The collective contributions of these interactions highlight the sophisticated molecular recognition mechanism employed by the 2'-dG-III riboswitch and provide insights into its ligand-binding specificity and stability.

Structure of 2'-dG-III riboswitch bound to guanosine and guanine, respectively

Previous research has indicated that the 2'-dG-III riboswitch exhibits comparable binding affinity toward 2'-dG, guanine, and guanosine (chemical structures depicted in Fig. 1A) [17]. To validate this observation, we conducted ITC experiments to measure the binding affinities. The results revealed that 2'dG-III riboswitch binds guanine with a dissociation constant $K_{\rm d}$ of 2.6 \pm 0.3 μ M, comparable to its binding affinity for 2'dG. In contrast, its affinity for guanosine was slightly lower, with a K_d of 4.6 \pm 0.1 μ M (Fig. 4D, Supplementary Fig. S2C– H, and Supplementary Table S3). To further elucidate the ligand recognition mechanism of the 2'-dG-III riboswitch binding to guanine and guanosine, we designed multiple constructs for crystallization. Among these, a variant of the WT riboswitch, named 2'-dG-III-D4 (Fig. 4A), in which four P1 base pairs were deleted, yielded high-quality crystals in its bound states with guanosine and guanine (Supplementary Table S2). The secondary structure of 2'-dG-III-D4 is illustrated in Fig. 4A, while the cartoon representations of 2'dG-III-D4 in complex with guanosine and guanine are displayed in Fig. 4B and C, respectively. To avoid confusion in the description, the corresponding nucleotide of 2'-dG-III-D4 is numbered same as the WT of 2'-dG-III riboswitch (Figs 1B and 4A). Notably, ITC measurements confirmed that the binding affinities of the 2'-dG-III-D4 construct for 2'-dG, guanosine, and guanine were comparable to those of the 2'dG-III WT construct (Fig. 4D, Supplementary Fig. S7A-C, and Supplementary Table S3). In addition to initial crystallization, we performed Mn²⁺-soaking experiments on the 2'-dG-III-D4-guanosine complex crystals to precisely map divalent metal ion positions using the anomalous signal from the Mn²⁺ replacements (Supplementary Table S3). Given the high quality of this crystal dataset, the subsequent structural analyses of the guanosine-bound state are based on this structure.

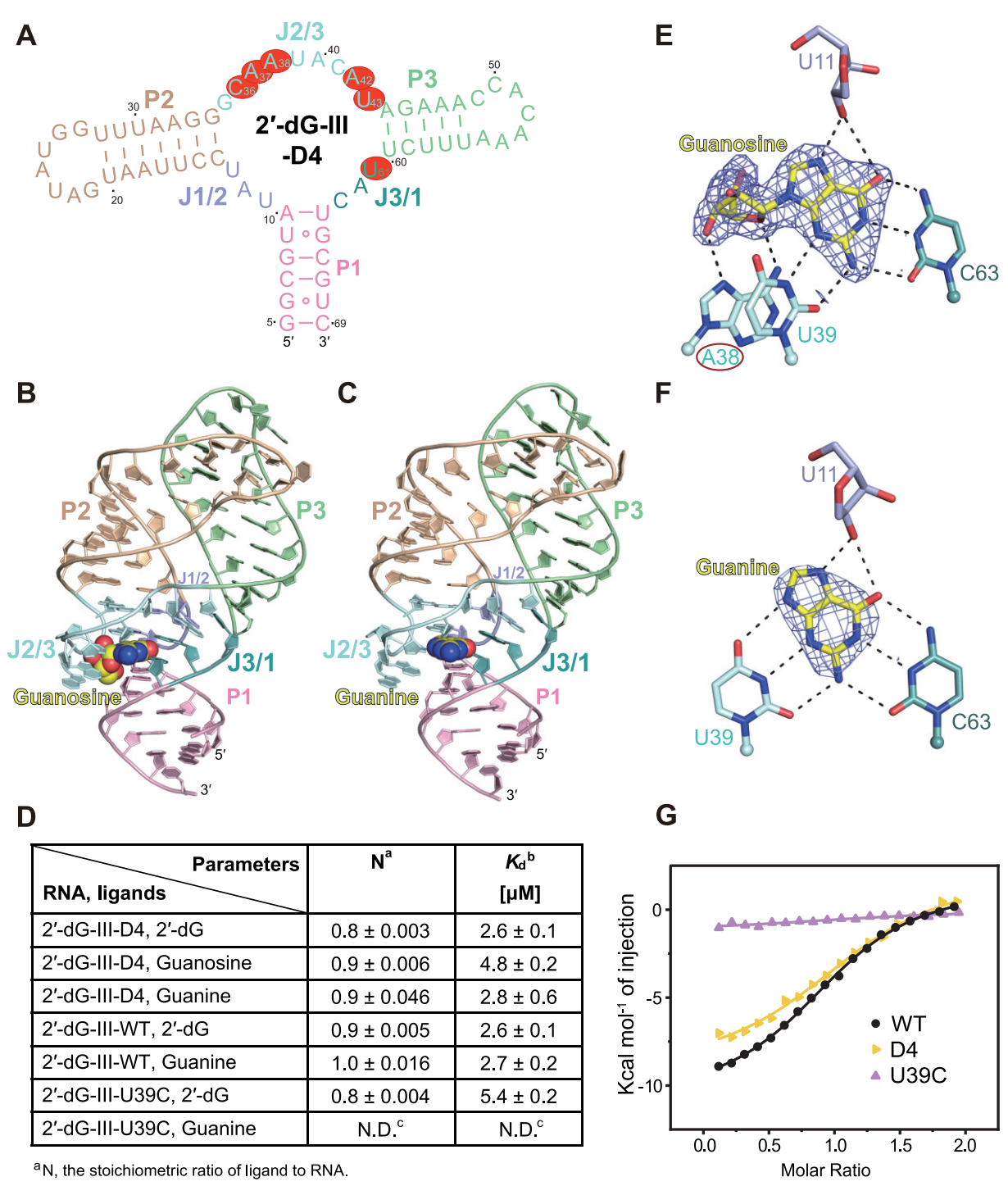
Structural alignment of the 2'-dG-III-D4 riboswitch bound to guanosine and guanine in PyMOL [26, 27] revealed a nearly identical overall tertiary folding, with a root mean square deviation of 0.515 Å (Supplementary Fig. S7D). However, subtle variations are observed in the base arrangement within the junction region, which may be attributed to the slight difference in crystal packing or the distinct ligand binding patterns of guanosine and guanine (Supplementary Fig. S7D and E). The interactions between the 2'-dG-III riboswitch in complex with guanosine are consistent with those observed for 2'-dG, in which both the bound 2'-dG and guanosine adopt 2'-endo sugar puck conformation (Figs 3C and 4E). Compared to 2'dG, 2'-OH of guanosine only forms a very weak hydrogen bond of 3.4 Å with O4 of U39 (Supplementary Fig. S7F). In the complex of 2'-dG-III-D4 riboswitch bound to guanine, the absence of ribose moiety in guanine enables guanine to adopt a unique binding mode (Fig. 4F). Within the binding pocket, guanine forms a Watson-Crick base pair with C63, while U11 establishes two hydrogen bonds with guanine's O6 and N7 atoms through its 2'-OH group (Fig. 4F). Additionally, U39 located near the sugar edge of the bound guanine, forms three hydrogen bonds with 2'-NH2, N3, and N9 atoms of guanine using its Watson-Crick edge. Together, U11, C63, and U39 encircle guanine from three sides, firmly anchoring it within the binding pocket (Fig. 4F). Although guanine lacks a ribose moiety, the formation of additional hydrogen bonds from the pairing interaction between the bound guanine and U39 may compensate for the absence of ribosemediated interactions observed in the 2'-dG-III riboswitch in complex with 2'-dG or guanosine (Figs 3C and 4E and F, and Supplementary Fig. S7F).

Based on these observations from the complex structures of 2'-dG-III riboswitch, we introduced a mutation into the 2'-dG-III riboswitch to explore the possibility of tuning its binding selectivity. Since U39 specifically pairs with the sugar edge of the bound guanine (Fig. 4F), we mutated U39 to C (U39C) to disrupt this pairing interaction and evaluated its binding affinity for both 2'-dG and guanine using ITC experiments. The results indicated that the U39C mutant retained a comparable binding affinity to 2'-dG as the WT, but completely lost its ability to bind guanine (Fig. 4D, Supplementary Fig. S7G and H, and Supplementary Table S3). Compared to 2'-dG-III-WT and 2'-dG-III-D4, our structure-guided U39C mutation successfully enhances the binding specificity of the 2'-dG-III riboswitch for 2'-dG over guanine (Fig. 4D and G), which is consistent with the observation that the corresponding nucleotides of U39 are cytosine in both the 2'-dG-I and 2'-dG-II riboswitches, wherein mutating cytosine to uridine reduces the 2'-dG binding affinity [18, 19].

Together, our findings highlight the remarkable adaptability of the 2'-dG-III riboswitch in recognizing structurally related purine ligands, demonstrating its capacity to adopt specific interactions that uniquely stabilize each ligand. Moreover, our results suggest that the binding specificity of the 2'-dG-III riboswitch can be fine-tuned through alterations of key interacting nucleotides. Determining and comparing its tertiary structure will further facilitate structure-guided rational mutagenesis to enhance ligand binding selectivity. This inherent flexibility in ligand recognition, coupled with the ability to modulate binding specificity, not only provides deeper insights into the functional dynamics of riboswitches but also expands their potential applications in synthetic biology, such as the design of engineered riboswitches for targeted gene regulation and biosensing.

Secondary structure and the junction core of Guanine-I and 2'-dG riboswitches

Three classes of 2'-dG riboswitches, termed 2'-dG-I, 2'-dG-II, and 2'-dG-III, have been identified from the variants of guanine riboswitch and exhibit high structural similarity to the Guanine-I riboswitch. All these riboswitches possess three stems (P1, P2, and P3), connected by an internal junction. Crystal structure analyses have revealed that they are characterized by a tuning fork-like scaffold [18, 19, 22] (Supplementary Figs S8A-S10A). In addition, long-distance interactions are formed between the top terminals of stems P2 and P3 in these structures (Supplementary Figs S3A and B, S8C and D, S9C and D, and S10C and D). Comparative analysis of the loop interactions reveals that two consecutive G-C base pairs are consistently formed in these four riboswitches (Supplementary Figs S3A and B, S8C and D, S9C and D, and S10C and D). Apart from these two G-C base pairs, 2'-dG-I adopts a distinct loop interaction pattern compared to Guanine-I, while 2'-dG-II and 2'-dG-III riboswitches share comparable loop interaction patterns, consistent with their similar loop sequences. In Guanine-I, 2'-dG-II, and 2'dG-III riboswitches, two consecutive base quadruplets were observed in each riboswitch: an upper U-G-C-A quadruplet (highlighted with light blue shadow) and a lower A-G-C-A quadruplet (highlighted with light yellow shadow), which are interconnected via specific A-G hydrogen bonds (A33-



^bThe binding disassociation parameter fitted for each independent titration.

Figure 4. The structures of 2'-dG-III riboswitch in complex with guanosine and guanine. (A) The secondary structure of the 2'-dG-III-D4, in which different regions are color-coded consistently with the corresponding regions shown in Fig. 1B. The nucleotides in the junction region that differ from those in the Guanine-I riboswitch are highlighted in red. Cartoon representation of the overall structure of 2'-dG-III-D4 riboswitch bound to guanosine (B) and guanine (C). (D) ITC-determined thermodynamic parameters of 2'-dG-III-D4, 2'-dG-III-WT, and 2'-dG-III-U39C binding to different ligands. The hydrogen bonding interactions and the composite omit maps (contoured at 1.0 σ level) of guanosine (E) and guanine (F) in the 2'-dG-III-D4 riboswitch binding pocket. The distinct mutated nucleotide A38 of Guanine-II riboswitch, which differs from the conserved nucleotide in the Guanine-I riboswitch, is framed in red. (G) Overlay of the fitted integrated heat plots obtained from ITC experiments evaluating the binding activity of 2'-dG-III-WT, 2'-dG-III-D4, and 2'-dG-III-U39C binding to guanine.

^cN.D. refers to no detectable interaction under the experiment conditions.

G37 in Guanine-I and 2'-dG-II riboswitches, and A22-G26 in the 2'-dG-III riboswitch) (Supplementary Figs S3A-F, S8C and D, and S10C and D). In contrast, the 2'-dG-I riboswitch adopts a completely distinct long-range interaction between the loops of stems P2 and P3, involving A71 intercalating between the consecutive bases A40-U41-A42 and forming a unique hydrogen-bonding network critical for regional stabilization (Supplementary Fig. S9C and D).

The ligand-binding cavities in these riboswitches are formed at the center of the junction region (Supplementary Figs S8B–S10B). Nucleotides within the junction regions form multiple base layers that tightly sandwich the bound ligand, involving both canonical Watson-Crick pairs (depicted as solid lines) and non-canonical pairs (depicted as dashed lines) (Fig. 5A-D). Comparative analysis of these binding pockets reveals distinct structural features among these riboswitches (Fig. 5A-C and Supplementary Figs S8E, S9E, and \$10E and F). Within the binding pocket of Guanine-I and 2'dG-I/II classes of riboswitches (Fig. 5A-C and Supplementary Figs S8E-S10E), a base triple is formed by a base pair at the apex of P1, along with a base from the J2/3 region, constituting the floor of the ligand-binding cavity (in light blue). In contrast, the floor of 2'-dG-III riboswitch binding pocket comprises the A10-U64 base pair at the apex of P1 (Fig. 5D and Supplementary Fig. S10F). In 2'-dG-II riboswitch (Fig. 5C and Supplementary Fig. S10E), the ceiling of the binding pocket (highlighted in purple) is formed by U22-A52-A77 base triple, in which U22-A52 constitutes a cis Watson-Crick base pair, and an additional hydrogen bond links A52 and A77. However, in Guanine-I, 2'-dG-I, and 2'-dG-III riboswitches, the ceilings are typical Watson-Crick base pairs (also highlighted in purple), specifically U22-A52 (Guanine-I), C31-G59 (2'-dG-I), and U11-A40 (2'-dG-III), respectively (Fig. 5A, B, and D, and Supplementary Figs S8E, S9E, and S10F). Notably, the layer above the ceiling consistently consists of an A-G-C base triple (highlighted in yellow) across all these riboswitches, including A23-G46-C53 in the Guanine-I riboswitch, A32-G53-C60 in 2'-dG-I, A23-G46-C53 in 2'-dG-II, and A12-G35-C41 in 2'-dG-III, respectively (Fig. 5 and Supplementary Figs S8E, S9E, and S10E and F).

Since the nucleotides that directly interact with the ligand within the binding pocket primarily determine the specificity of ligand recognition, we performed a detailed comparison of these interactions in the riboswitches. Unlike adenine riboswitches, which employ a conserved uridine for ligand binding [14], Guanine-I and 2'-dG-I/II/III riboswitches, originating from the guanine riboswitch family, rely on a highly conserved cytosine to recognize the Watson-Crick edge of the guanine moiety in their respective ligands. In addition, these riboswitches all utilize 2'-OH of specific nucleotides (U22 in Guanine-I riboswitch, C31 in 2'-dG-I riboswitch, U22 in 2'dG-II riboswitch, and U11 in 2'-dG-III riboswitch) to interact with the Hoogsteen edge of the guanine moiety (Fig. 5). Different sugar edge recognition modes of the bound guanine have been identified in these riboswitches. Guanine-I and 2'-dG-III riboswitches utilize one uridine (Fig. 5A and D), whereas 2'-dG-I and 2'-dG-II riboswitches employ one cytosine (Fig. 5B and C). Among the three 2'-dG riboswitch classes, the attached sugar moiety of the bound 2'-dG is also specifically recognized. Notably, 2'-dG-III riboswitch exhibits a distinct recognition pattern involving A38, whereas 2'-dG-I and 2'-dG-II riboswitches share a similar recognition pattern involving one cytosine and the 2'-OH of another nucleotide (Fig. 5B-D).

Comparative analysis of these riboswitches, along with previous studies, suggests that the ligand binding affinity and specificity can be modulated by modifying other nucleotides involved in ligand interaction. A38 is one of the distinctive featured nucleotides in 2'-dG-III riboswitch (Fig. 1B and D, and Supplementary Fig. S1B and C), which is also involved in the specific recognition of the sugar moiety of 2'-dG and guanosine (Figs 3C and 4E). Our ITC experiments revealed that A38C mutant exhibited an increased binding affinity for 2'-dG, with a K_d of 0.8 \pm 0.02 μ M, compared to the WT (Fig. 3D, Supplementary Fig. S6D, and Supplementary Table S3). To further investigate the impact of the A38C mutation on ligand binding, we performed ITC experiments to assess its affinity for guanine. Notably, the mutant also showed an enhanced binding affinity for guanine, with a K_d of 1.9 \pm 0.4 μM (Supplementary Fig. S6E and Supplementary Table S3). Although A38C mutant enhanced binding affinity for both ligands, the improvement was more pronounced for 2'-dG, suggesting A38C mutation not only improves binding capacity but also refines ligand selectivity. This intricate interplay of nucleotide arrangements and interactions enables riboswitches to achieve effective and selective binding to their target ligands, highlighting their versatility and potential applications in synthetic biology.

Design of a sensor for 2'-dG detection based on the structure of 2'-dG-III riboswitch

In recent years, extensive studies of RNA fluorogenic aptamers, such as Spinach, Pepper, and Clivia, have greatly advanced the development of RNA-based biosensors [28–32]. Riboswitches typically exhibit high specificity for their corresponding ligands and fusing riboswitches with fluorogenic aptamers enables real-time detection of dynamic changes in ligand levels via fluorescence signals. Compared to other riboswitch families, the 2'-dG-III riboswitch displays relatively lower binding specificity for its cognate ligand. Based on our detailed investigation of its ligand-binding pocket and recognition patterns, we sought to engineer the 2'-dG-III riboswitch to develop a 2'-dG-specific biosensor with enhanced ligand-binding specificity for sensitive detection of dynamic 2'-dG fluctuations.

Pepper is a fluorogenic RNA aptamer ble of binding to the small molecule dye, (4-((2-hydroxyethyl)(methyl)amino)-benzylidene)cyanophenylacetonitrile), and enhancing its fluorescence by over 3000-fold [33, 34]. Based on the crystal structures and working mechanisms of both Pepper aptamer and 2'dG-III riboswitch, we engineered a fusion RNA construct by integrating the stem P1 of the 2'-dG-III riboswitch with stem P1 of the Pepper aptamer, forming a continuous helical element essential for sensor function (Fig. 6A). In this design, the 2'-dG-III riboswitch serves as the sensing module to detect ligands. Upon ligand binding, the RNA sensor undergoes a rapid conformational rearrangement that promotes the proper folding of the Pepper aptamer, enabling it to bind HBC and produce a strong fluorescence signal (Supplementary Fig. S11A).

To optimize the length of the fusing stem for achieving a highly sensitive fluorescence response, we systematically tested various base pair combinations and evaluated the

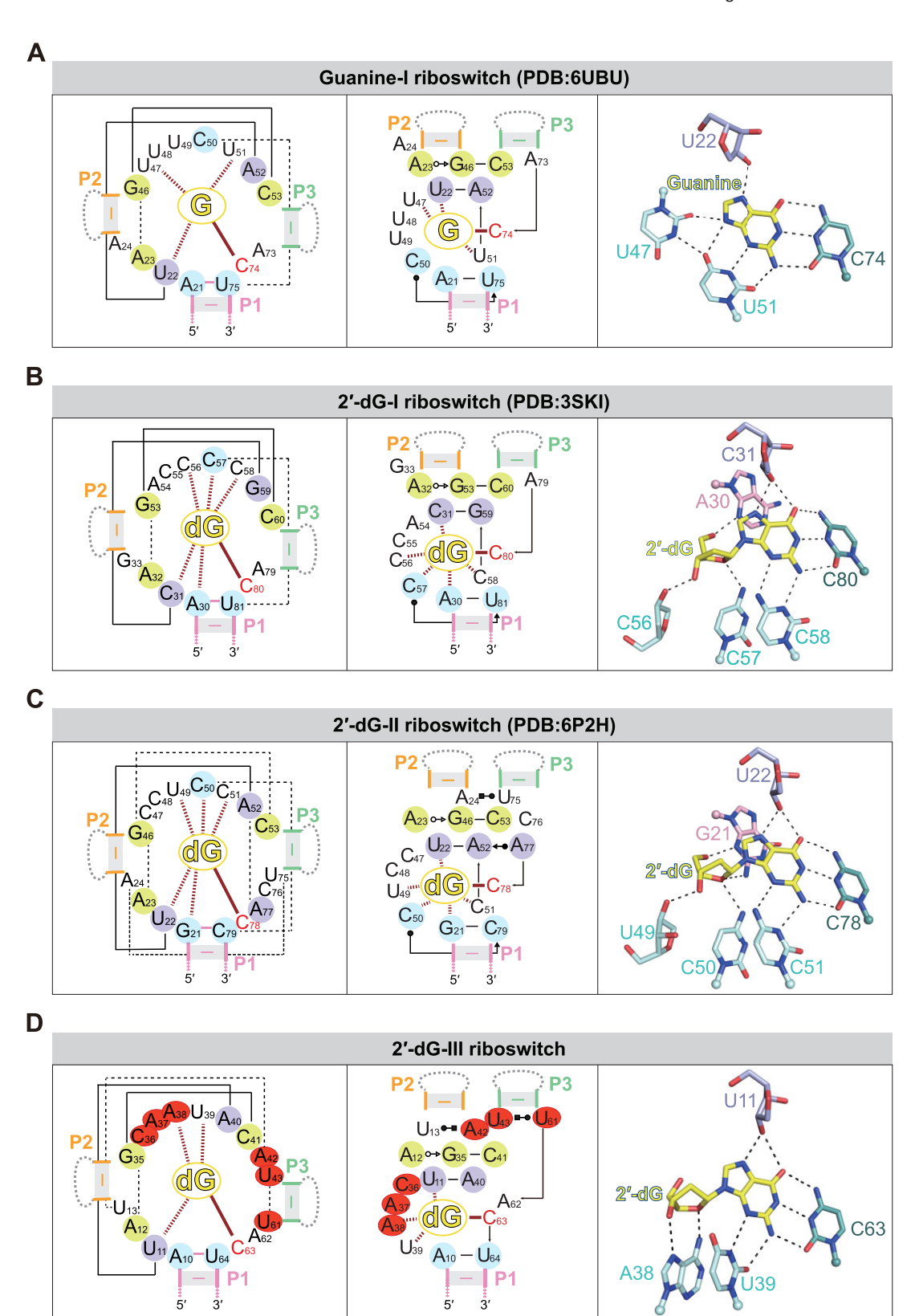


Figure 5. Details of long-range interactions and binding pockets in Guanine-I and 2'-dG-I/II/III riboswitches. The secondary structures and schematic representations of the junctions, and binding pocket compositions of the Guanine-I riboswitch (A), 2'-dG-I riboswitch (B), 2'-dG-II riboswitch (C), and 2'-dG-III riboswitch (D) are shown. In the secondary structure, standard Watson–Crick base pairs are depicted using solid lines, whereas non-Watson–Crick base pairs are represented using the Leontis–Westhof nomenclature. Interactions between the ligand and involved nucleotides are indicated with red lines, while other hydrogen bonds are depicted in black. The first layer of nucleotides beneath the ligand is colored light blue, and the first and second layers above the ligand are colored purple and yellow, respectively. Additionally, the nucleotides in the 2'-dG-III riboswitch junction region that differ from those in the Guanine-I riboswitch are highlighted in red.

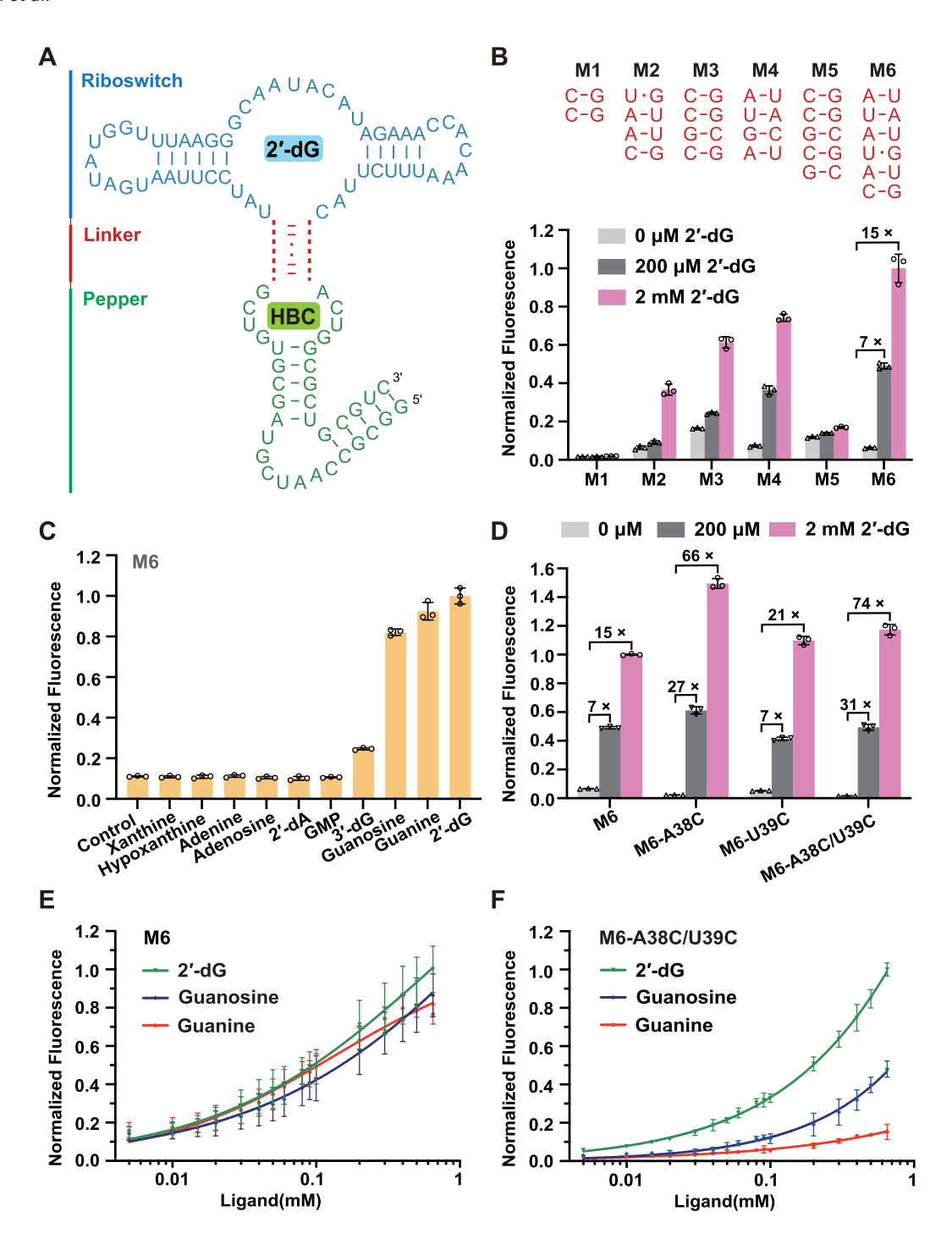


Figure 6. Fluorescence assay of the 2'-dG RNA sensor. (A) The secondary structure of the fusion RNA, where the 2'-dG-III riboswitch (in blue) and the Pepper aptamer (in green) are connected by a variable linker region (in red). The linker region was systematically investigated with different base pair combinations to optimize the sensor's performance. (B) The compositions of the linker regions (M1–M6) and their corresponding fluorescence assays. Among these tested linkers, M6 exhibited the lowest background fluorescence and the highest sensitivity to 2'-dG, making it the optimal variant for the sensor design. The activated fluorescence of HBC in these sensors, measured in three independently repeated experiments, was normalized for comparison with M6 in 2 mM 2'-dG. (C) Fluorescence assay of the M6 sensor to different purine ligands. The sensor exhibited moderate fluorescence in response to guanosine, guanine, and 2'-dG. The fluorescence of HBC was measured in three independent experiments and normalized for comparison with the results obtained in 200 μ M 2'-dG. Data are presented as the mean \pm standard deviation (SD) of three replicates. (D) Fluorescence assay of M6 and M6-related mutants with 2'-dG. The fluorescence intensity of HBC was normalized for comparison with that of M6 in the presence of 2 mM 2'-dG. Fluorescence assays of the M6 (E) and M6-A38C/U39C (F) with 2'-dG, guanosine, and guanine. Data are presented as the mean \pm SD from three replicates.

corresponding fluorescence across a range of 2'-dG concentrations. Among the tested constructs, the variant containing six base pairs in the fusion stem, designed as M6 (Fig. 6A and B), exhibited the best performance. M6 shows minimal background fluorescence in the absence of 2'-dG, while producing a robust fluorescence increase in response to the rising 2'-dG concentrations (Fig. 6B). We further evaluated the specificity of M6 by testing its response to other purine ligands. The results showed negligible activation by oxidized purine analogs such as xanthine and hypoxanthine, as well as adenine-based compounds including adenine, adenosine, and 2'-dA (Fig. 6C), consistent with the known ligand selectivity of the 2'-dG-III riboswitch. Among guanine-containing analogs, M6 exhibited the strongest fluorescence response to 2'-dG, a slightly weaker response to guanosine and guanine, and the lowest response to 3'-dG and GMP (Fig. 6C). This ligand discrimination likely reflects the highly specific structural composition of the riboswitch binding pocket, which selectively accommodates ligands based on subtle molecular differences.

To improve the ligand specificity of M6, we focused on modulating the key nucleotides within the binding pocket of 2'-dG-III riboswitch. As previously described, the U39C mutation significantly improved ligand specificity for 2'-dG (Fig. 4D, Supplementary Fig. S7G and H, and Supplementary Table S3), while the A38C mutation not only increased binding affinity for 2'-dG but also enhanced specificity (Fig. 3D, Supplementary Fig. S6D and E, and Supplementary Table S3). Based on these findings, we introduced the single mutations (U39C and A38C) as well as a double mutation (A38C/U39C) into the M6 construct and assessed their fluorescence responses across a range of 2'-dG concentrations. As shown in Fig. 6D, M6-U39C exhibited no significant improvement in fluorescence response, likely due to its similar binding affinity for 2'-dG as the WT (Fig. 4D, Supplementary Fig. S7G, and Supplementary Table S3). In contrast, both M6-A38C and M6-A38C/U39C showed markedly enhanced fluorescence signals at 200 µM and 2 mM 2'-dG, with M6-A38C/U39C displaying the most pronounced increase (Fig. 6D).

Furthermore, we evaluated the ligand discrimination capabilities of the mutant RNA sensors by comparing their fluorescence responses to 2'-dG, guanosine, and guanine (Supplementary Fig. S11B). The results showed that M6-A38C exhibited reduced fluorescence responses of 28% and 70% for guanosine and guanine, respectively, compared to 2'dG. M6-U39C displayed significantly reduced fluorescence responses to these analogs, with only 50% and 43% for guanosine and guanine, respectively. Notably, the double mutant M6-A38C/U39C exhibited a dramatic fluorescence reduction in response to guanine, down to 19% of that for 2'-dG, while its response to guanosine remained at 47% relative to 2'dG. We further evaluated the fluorescence responses of M6 and M6-A38C/U39C across a range of ligand concentrations (Fig. 6E and F). M6 showed similar response values for 2'dG, guanosine, and guanine at all tested concentrations, indicating poor ligand discrimination (Fig. 6E). In contrast, M6-A38C/U39C consistently produced the strongest fluorescence response to 2'-dG, with enhanced specificity at higher ligand concentrations (Fig. 6F). Consistent with these findings, ITC titration of the A38C/U39C mutant of 2'-dG-III riboswitch exhibited an eight-fold decrease in binding affinity for guanine compared with 2'-dG (Supplementary Fig. S11C and D). Together, these results demonstrate that the A38C/U39C double mutation synergistically fine-tunes the selectivity of the 2'-dG-

III riboswitch and enhances sensor performance by maintaining strong responsiveness to 2'-dG while substantially reducing non-specific recognition of related purine analogs.

Concluding remarks

The 2'-dG-III riboswitch originates from the guanine family, featuring distinct mutations and insertions in the central junction region of the common guanine riboswitch motif, which enable 2'-dG-III riboswitch to possess a unique junction composition (Figs 1 and 5). Through comparative analysis of the 2'-dG-III riboswitch with guanine-I and 2'dG-I/II riboswitches (Fig. 5 and Supplementary Figs S3 and S7–S9), we deciphered the unique folding patterns of these guanine riboswitch variants and uncovered the potential finetuning principles governing their ligand recognition. The tertiary structure of 2'-dG-III riboswitch in complex with 2'dG, guanosine, and guanine (Figs 1E and 4B and C) reveals 2'-dG-III riboswitch maintains the characteristic tuningfork-like scaffold typical of guanine family riboswitches, with long-distance interactions forming between stems P2 and P3. Within the binding pocket, although the 2'-dG-III riboswitch shares some common guanine-base recognition patterns with other guanine riboswitch variants, including Guanine-I, 2'dG-I, and 2'-dG-II, it adopts a unique sugar moiety recognition mode through A38 (Figs 3C and 4E, and Supplementary Fig. S1B and C). Consistent with this observation, A38 is one of the distinct mutated nucleotides in the 2'-dG-III riboswitch (Supplementary Fig. S1B). In addition to A38, another distinct mutated nucleotide, A37, forms a supporting platform beneath A38, thereby strengthening the interaction between A38 and the bound ligand, while C36 contributes flexibility to shape the binding pocket within the junction (Fig. 2A and Supplementary Fig. S1B and C). The three distinct inserted nucleotides, A42, U43, and U61, form extensive crosstalk interactions within the junction, providing a unique supportive platform for stems P2 and P3 located above the binding pocket (Fig. 2A-D and Supplementary Fig. S10F). The structure-based investigation not only enhances our understanding of how minor structural variations can shape the overall structure and influence ligand recognition specificity, but also enables the precise classification of riboswitch families among closely related riboswitch variants.

Structural analyses of the tertiary folds and the composition of the ligand binding pockets reveal that, while 2'-dG-I and 2'-dG-II riboswitches share common ligand interaction patterns, the 2'-dG-III riboswitch features a distinct binding pocket composition and a unique ligand recognition mode, resulting in different binding characteristics (Fig. 5). Compared to the higher binding specificities of 2'-dG-I and 2'-dG-II riboswitches [15, 16, 19, 20], 2'-dG-III riboswitch exhibits relatively lower specificity, showing similar binding affinities to guanine, guanosine, and 2'-dG [17] (Fig. 4D). To further investigate potential ligands of the 2'-dG-III riboswitch, we examined 2'-dGMP (Supplementary Fig. S11E). However, our ITC experiments indicate that the 2'-dG-III riboswitch does not bind to 2'-dGMP (Supplementary Fig. S11E), likely due to steric hindrance caused by the phosphate group. These results suggest that while the 2'-dG-III riboswitch tolerates certain structural variations in guanine derivatives, it maintains stringent selectivity for optimal ligands. These differences in binding specificity among the three 2'-dG riboswitches may be related to their respective functions. Functionally, 2'-dG-I

and 2'-dG-II riboswitches regulate gene expression via transcription termination, controlling genes involved in processes such as ribonucleotide reduction and phosphate transport [15, 16]. Their strict response to deoxyribonucleoside concentrations likely reflects the necessity for precise regulatory control. In contrast, the 2'-dG-III riboswitch, located exclusively upstream of purine nucleoside hydrolase genes, exhibits broader ligand recognition and likely plays a more global regulatory role in purine metabolism [17]. When intracellular concentrations of guanine-containing ligands rise sufficiently, the 2'-dG-III riboswitch will bind to these ligands and activate nucleoside hydrolase expression. The distinct regulatory mechanism of the 2'-dG-III riboswitch likely reflects its differing role in maintaining purine homeostasis.

In the guanine riboswitch family, the binding pockets are constituted by the nucleotides located in the internal junctions. Previous studies indicate that alterations of these nucleotides can fine-tune the binding affinity and specificity for various ligands [18, 19, 35]. For instance, mutating U51 to C in the Guanine-I riboswitch significantly enhances its affinity for 2'-dG while reducing its affinity for guanine [35]. Similarly, mutations of C58 and C51 to U in the 2'-dG-I and 2'-dG-II riboswitches, respectively, lead to a notable decrease in their affinity for 2'-dG [18, 19]. Comparative analysis of 2'-dG-III riboswitch complexes bound with different related ligands, such as 2'-dG, guanosine, and guanine, as well as comparisons with Guanine-I and 2'-dG-I/II riboswitches (Fig. 5 and Supplementary Figs S8-S10), reveals that the 2'dG-III riboswitch possesses structural plasticity to accommodate specific ligands, prompting us to fine-tune the binding specificities through subtle changes in the binding pocket (Figs 3C and 4E and F). The U39C mutation, which involves the guanine sugar edge recognition, retained binding affinity for 2'-dG but completely lost the ability to bind guanine (Supplementary Fig. S7G and H, and Supplementary Table S3). The A38C mutation in the 2'-dG-III riboswitch, which affects sugar moiety recognition of both 2'-dG and guanosine, enhances ligand binding affinity and improves selectivity for 2'-dG over guanine. (Supplementary Fig. S6D and E, and Supplementary Table S3). These structure-based subtle alterations in the binding pocket composition fine-tune the binding affinity and specificity of the 2'-dG-III riboswitch, reaffirming that ligand recognition in riboswitches can be modulated through binding pocket modifications. Given that several new riboswitch classes have been identified from the guanine riboswitch variants, these fine-tuning principles also provide valuable insights for discovering new riboswitch classes within the existing guanine riboswitch family.

The unique biochemical properties of RNA molecules make them excellent scaffolds for biosensor construction. Based on our findings, we developed a 2'-dG-III riboswitch-based RNA biosensor suitable for the detection of 2'-dG by fusing the WT 2'-dG-III riboswitch (serving as the sensing module) with the Pepper fluorescent aptamer (serving as the signaling module) (Fig. 6 and Supplementary Fig. S11). Among the various designs tested, M6 construct containing a six-base-pair connecting stem exhibited the most robust fluorescence response to 2'-dG, highlighting the critical importance of the connecting element. In RNA biosensor design, the structural linkage plays a pivotal role in facilitating efficient allosteric communication, which ensures that ligand binding to the riboswitch properly triggers the folding and fluorescence activation of the fluorogenic aptamer. Our results emphasize that the precise selection

and optimization of this fusion interface is essential for functional RNA sensor construction. Moreover, this strategy provides a broad approach for enhancing the signal transduction efficiency of RNA-based biosensors, offering new avenues for their rational design and expanded applications.

To improve sensor performance, we incorporated the confirmed fine-tuning mutations (A38C and U39C) of the 2'dG-III riboswitch into the sensor module to enhance its specificity and sensitivity toward 2'-dG. Notably, the double mutant A38C/U39C generated a significantly enhanced fluorescence response to 2'-dG across various concentrations while markedly reducing non-specific binding to other purine analogs, such as guanosine and guanine (Fig. 6E and F, and Supplementary Fig. S11B). These results not only establish a solid foundation for the development of highly specific nucleic acid sensors, but also demonstrate the potential of rationally engineered riboswitches in biosensing applications. However, since our current investigation was conducted *in vitro*, further studies are necessary to evaluate the performance and applicability of this sensor system in more complex biological environments, including live-cell and in vivo contexts. Exploring these aspects will be crucial for advancing the practical use of RNA-based biosensors in biomedical and diagnostic applications.

Acknowledgements

We thank the staff members of the Large-scale Protein Preparation System, BL-17B, BL-17U1, BL18U1, BL-19U1, and BL02U1 beamlines at the National Facility for Protein Science in Shanghai (NFPS), Zhangjiang Lab, China for providing technical support and assistance in data collection and analysis. We thank the staff of the BL02U1 beamline at the National Center for Protein Sciences Shanghai (NCPSS) at SSRF for their assistance in X-ray data collection. We thank the technical assistance from the core facility of the Life Sciences Institute (LSI), Zhejiang University.

Author contributions: Xin Shen (Formal analysis [equal], Investigation [equal], Methodology [equal], Validation [equal], Writing—original draft [equal]), Hongcheng Li (Investigation [equal]), Aiming Ren (Conceptualization [lead], Project administration [lead], Supervision [lead], Validation [lead]), Qianqian Song (Methodology [supporting]), Xiaoqing Tai (Formal analysis [supporting]), and Mengqi He (Methodology [supporting]).

Supplementary data

Supplementary data is available at NAR online.

Conflict of interest

None declared.

Funding

This work was supported by the National Natural Science Foundation of China [32325029, 91940302, and 91640104 to A.R.], Zhejiang Provincial Natural Science Foundationof China [LD25C050002 to A.R.], and the National Key Research and Development Project of China [2023YFC2604300 and 2021YFC2300300 to A.R.]. Funding to pay the Open Ac-

cess publication charges for this article was provided by Zhejiang University.

Data availability

Atomic coordinates and structure factors for 2'-dG-III riboswitch in complex with 2'-dG, guanosine, and guanine have been deposited with the Protein Data bank (www.rcsb. org) under accession numbers 9LKV, 9LKU, 9UW0 (Mn²⁺-soaked), and 9LKW, respectively. All study data are included in the article and/or Supplementary data.

References

- Sudarsan N, Barrick JE, Breaker RR. Metabolite-binding RNA domains are present in the genes of eukaryotes. RNA 2003;9:644–7. https://doi.org/10.1261/rna.5090103
- 2. Kavita K, Breaker RR. Discovering riboswitches: the past and the future. *Trends Biochem Sci* 2023;48:119–41. https://doi.org/10.1016/j.tibs.2022.08.009
- 3. Breaker RR. Prospects for riboswitch discovery and analysis. *Mol Cell* 2011;43:867–79. https://doi.org/10.1016/j.molcel.2011.08.024
- Garst AD, Edwards AL, Batey RT. Riboswitches: structures and mechanisms. Cold Spring Harb Perspect Biol 2011;3:a003533. https://doi.org/10.1101/cshperspect.a003533
- Breaker RR. Riboswitches and the RNA world. Cold Spring Harb Perspect Biol 2012;4:a003566. https://doi.org/10.1101/cshperspect.a003566
- Serganov A, Nudler E. A decade of riboswitches. Cell 2013;152:17–24. https://doi.org/10.1016/j.cell.2012.12.024
- De Lay NR, Garsin DA. The unmasking of 'junk' RNA reveals novel sRNAs: from processed RNA fragments to marooned riboswitches. *Curr Opin Microbiol* 2016;30:16–21. https://doi.org/10.1016/j.mib.2015.12.006
- 8. Jones CP, Ferre-D'Amare AR. Long-range interactions in riboswitch control of gene expression. *Annu Rev Biophys* 2017;46:455–81.
- https://doi.org/10.1146/annurev-biophys-070816-034042
- Bedard AV, Hien EDM, Lafontaine DA. Riboswitch regulation mechanisms: RNA, metabolites and regulatory proteins. *Biochim Biophys Acta Gene Regul Mech* 2020;1863:194501. https://doi.org/10.1016/j.bbagrm.2020.194501
- Micura R, Höbartner C. Fundamental studies of functional nucleic acids: aptamers, riboswitches, ribozymes and DNAzymes. *Chem* Soc Rev 2020;49:7331–53. https://doi.org/10.1039/D0CS00617C
- Breaker RR. The biochemical landscape of riboswitch ligands. Biochemistry 2022;61:137–49. https://doi.org/10.1021/acs.biochem.1c00765
- Antunes D, Santos LHS, Caffarena ER et al. Bacterial 2'-deoxyguanosine riboswitch classes as potential targets for antibiotics: a structure and dynamics study. Int J Mol Sci 2022;23:1925. https://doi.org/10.3390/ijms23041925
- Pedley AM, Benkovic SJ. A new view into the regulation of purine metabolism: the purinosome. *Trends Biochem Sci* 2017;42:141–54. https://doi.org/10.1016/j.tibs.2016.09.009
- Mandal M, Breaker RR. Adenine riboswitches and gene activation by disruption of a transcription terminator. *Nat Struct Mol Biol* 2004;11:29–35.
- 15. Kim JN, Roth A, Breaker RR. Guanine riboswitch variants from mesoplasma florum selectively recognize 2'-deoxyguanosine. Proc Natl Acad Sci USA 2007;104:16092-7. https://doi.org/10.1073/pnas.0705884104
- Weinberg Z, Nelson JW, Lünse CE et al. Bioinformatic analysis of riboswitch structures uncovers variant classes with altered ligand

- specificity. *Proc Natl Acad Sci USA* 2017;**114**:E2077–85. https://doi.org/10.1073/pnas.1619581114
- 17. Hamal Dhakal S, Panchapakesan SSS, Slattery P et al. Variants of the guanine riboswitch class exhibit altered ligand specificities for xanthine, guanine, or 2'-deoxyguanosine. Proc Natl Acad Sci USA 2022;119:e2120246119. https://doi.org/10.1073/pnas.2120246119
- Pikovskaya O, Polonskaia A, Patel DJ et al. Structural principles of nucleoside selectivity in a 2'-deoxyguanosine riboswitch. Nat Chem Biol 2011;7:748–55. https://doi.org/10.1038/nchembio.631
- 19. Matyjasik MM, Batey RT. Structural basis for 2'-deoxyguanosine recognition by the 2'-dG-II class of riboswitches. *Nucleic Acids Res* 2019;47:10931–41. https://doi.org/10.1093/nar/gkz839
- Pikovskaya O, Serganov AA, Polonskaia A et al. Preparation and Crystallization of Riboswitch-Ligand Complexes. In: Serganov A (ed.), Riboswitches: Methods and Protocols. Totowa, NJ: Humana Press, 2009, 115–28.
- 21. Kabsch W. XDS. Acta Crystallogr D Biol Crystallogr 2010;66:125–32. https://doi.org/10.1107/S0907444909047337
- 22. Serganov A, Yuan Y-R, Pikovskaya O *et al.* Structural basis for discriminative regulation of gene expression by adenine- and guanine-sensing mRNAs. *Chem Biol* 2004;11:1729–41.
- 23. Collaborative Computational Project, Number 4. The CCP4 suite: programs for protein crystallography. *Acta Crystallogr D Biol Crystallogr* 1994;50:760–3. https://doi.org/10.1107/S0907444994003112
- 24. Emsley P, Lohkamp B, Scott WG *et al.* Features and development of Coot. *Acta Crystallogr D Biol Crystallogr* 2010;66:486–501. https://doi.org/10.1107/S0907444910007493
- 25. Adams PD, Afonine PV, Bunkóczi G *et al.* PHENIX: a comprehensive Python-based system for macromolecular structure solution. *Acta Crystallogr D Biol Crystallogr* 2010;66:213–21. https://doi.org/10.1107/S0907444909052925
- 26. Schrodinger LLC. The PyMOL Molecular Graphics System, Version 3.1.0. 2010. https://www.pymol.org/
- 27. Mura C. Development & implementation of a PyMOL 'putty' representation. arXiv, https://doi.org/10.48550/arXiv.1407.5211, 19 July 2014, preprint: not peer reviewed.
- 28. Fowler CC, Li Y. Construction and application of riboswitch-based sensors thatdetect metabolites within bacterial cells. In: Lafontaine D, Dubé A (eds.), *Therapeutic Applications of Ribozymes and Riboswitches*. Totowa, NJ: Humana Press, 2014, 177–97. https://doi.org/10.1007/978-1-62703-730-3 14
- Chen Z, Chen W, Reheman Z et al. Genetically encoded RNA-based sensors with Pepper fluorogenic aptamer. Nucleic Acids Res 2023;51:8322–36. https://doi.org/10.1093/nar/gkad620
- 30. Wang TH, Simmel FC. Switchable fluorescent light-up aptamers based on riboswitch architectures. *Angew Chem Int Ed Engl* 2023;62:e202302858.
- Chen Z, Chen W, Xu C et al. Near-infrared fluorogenic RNA for in vivo imaging and sensing. Nat Commun 2025;16:518. https://doi.org/10.1038/s41467-024-55093-1
- Wu Y, Kong W, Van Stappen J et al. Genetically encoded fluorogenic DNA aptamers for imaging metabolite in living cells. J Am Chem Soc 2025;147:1529–41. https://doi.org/10.1021/jacs.4c09855
- 33. Huang K, Chen X, Li C *et al.* Structure-based investigation of fluorogenic Pepper aptamer. *Nat Chem Biol* 2021;17:1289–95. https://doi.org/10.1038/s41589-021-00884-6
- 34. Chen X, Zhang D, Su N et al. Visualizing RNA dynamics in live cells with bright and stable fluorescent RNAs. Nat Biotechnol 2019;37:1287–93. https://doi.org/10.1038/s41587-019-0249-1
- 35. Edwards AL, Batey RT. A structural basis for the recognition of 2'-deoxyguanosine by the purine riboswitch. *J Mol Biol* 2009;385:938–48. https://doi.org/10.1016/j.jmb.2008.10.074